Asian Journal of Chemistry; Vol. 29, No. 9 (2017), 1873-1878

ASIAN JOURNAL OF CHEMISTRY

https://doi.org/10.14233/ajchem.2017.20687

REVIEW

Modifications of ZnO Interlayer to Improve the Power Conversion Efficiency of Organic Photovoltaic Cells

DIVYA JAYARAM*, ADITI GOYAL, DURVA NAIK, PRERNA GOSWAMI and M.A.K. KERAWALLA

Department of Polymer Engineering and Surface Coatings Technology, Institute of Chemical Technology, Mumbai-400 019, India

*Corresponding author: E-mail: divyajayaram98@gmail.com

Received: 5 April 2017; *Accepted*: 31 May 2017; *Published online*: 15 July 2017; AJC-18457

Power conversion efficiency (PCE) is an important parameter in determining the performance of organic photovoltaics (OPVs). Various factors lead to enhancement of power conversion efficiency. One such factor is doping of electron transport layer. A substantial increase in the power conversion efficiency of inverted organic solar cells is realized by a ZnO doped buffer layer acting as an electron-transport layer. Different works on Li, Cd, Ga, Al doping, introduction of C60 interface layer in ZnO buffer layer and dual doped system of InZnO-BisC60 have been reviewed here. The Al-doped buffer layer device showed the highest increase in power conversion efficiency.

Keywords: Organic photovoltaics, Doping, Power conversion efficiency, ZnO interlayer.

INTRODUCTION

Deficit of energy has been one of the leading problems faced by humanity for a long time [1]. This has led to a rise in understanding and development of complementary set of sustainable energies [2]. Solar energy is one such source that is being harvested. Extensive research in the field of solar energy has led to developments in inorganic and organic photovoltaic cells. A photovoltaic cell (PVC) is a specialized semiconductor diode that converts light energy to electrical energy, in the form of direct current. Conventional and dominating classical crystalline inorganic silicon solar modules now receive competition from organic photovoltaic cells (OPVs) [3].

Organic photovoltaics use organic electronics: A branch of material science dealing with small organic molecules and polymers having conductive properties. They are composed of a film of organic photovoltaic active layer, which is sandwiched between a transparent electrode and a metal electrode [4]. The active layer of organic photovoltaic device is composed of conjugated systems, which constitute the donor while the acceptor is usually fullerene.

Polymer solar cells mostly are composed of an electron- or hole-blocking layer on top of an indium tin oxide (ITO) conductive glass followed by an electron donor and an electron acceptor. The order as well as the nature of the blocking layers and that of the metal electrode–depends on the device architecture. In an inverted cell, the electric charges exit the device in an opposite direction as compared to that in a normal device [5,6]. The reason behind this is the reversing of positive and negative electrodes (which absorb the negative and positive charges, respectively) .

There have been numerous investigations of polymer solar cells (PSCs) with an inverted device structure using modified indium tin oxide (ITO) as the cathode [7]. Compared with conventional PSCs, inverted devices are known to exhibit long term stability by avoiding the need for the corrosive and hygroscopic hole-transporting poly(3,4-ethylenedioxylene-thiophene):poly-(styrene sulphonic acid) (PEDOT:PSS) and low work function metal cathode, both of which decrease the device lifetime [8,9]. Moreover, inverted PSCs can also take advantage of the con-centration gradient and the vertical phase separation in the active layer reason being the air-stable metals that are used as the top electrode [9,10]. Therefore, an ideal configuration for all types of PSCs is the inverted device structure.

Over the traditional inorganic PVCs, organic photovoltaics have advantages such as low cost of production, high flexibility, transparency of the device and the ease of design. Moreover, the optical absorption capacity of organic molecules is high, so a large amount of light is absorbed with a small amount of material [11]. This has allowed their integration into building components for a variety of applications [12] and has gained the general attention because of the possibility of developing economical devices [13].

However, the major drawback of organic photovoltaics is low efficiency, lack of stability and low strength as compared to inorganic PVCs [14]. Owing to state of the art technology, power conversion efficiencies of 10-15 % have been predicted [15]. This value is significantly lower than that of inorganic PVCs. It is mainly due to the fact that organic semiconductors have a much higher band gap as compared to inorganic semiconductors. The light absorption in organic photovoltaics result in the formation of excitons rather than free electrons and holes. Due to this fundamental difference, the process involved in the conversion of photons into electrical energy is not the same as that occurring in inorganic PVCs [11]. The small exciton diffusion lengths and low carrier mobilities result in low efficiency.

Conversion of light to electricity in organic photovoltaics is carried out by the following processes: (a) Light absorption (b) Exciton formation and diffusion (c) Exciton dissociation into free charge carriers (d) Charge transport (e) Charge collection by the electrodes.

Efficiency improvement can therefore be achieved by enhancing the efficiencies of these processes in organic solar cells [16].

In the past decade, rigorous research has been carried out to study the influence of a wide range of factors on power conversion efficiencies of photovoltaics to overcome the problem of low efficiency. One such parameter is the donor-acceptor pair used. Using different types of polymer donors leads to variation in power conversion efficiency [17,18]. Enhanced organic photovoltaic cell (OPV) efficiency has been obtained through the use of continuously graded donor–acceptor (D–A) heterojunctions. Device performance is a strong function of both D–A grading and overall composition ratio [19].

Chemical doping, which controls the conductivity of organic thin films, can greatly enhance power conversion of organic photovoltaics [20]. Power conversion efficiency (PCE) of 9.2 % has been obtained in single junction polymer solar cells in addition to the remarkable progress in designing of low band gap polymers. A power conversion efficiency of 10.6 % has been achieved in a tandem structure [21,22].

Design factors, like transparency and thickness are also known to affect the power conversion efficiency of organic photovoltaics. Yu *et al.* [23] have studied the influence of device structures on power conversion efficiency, among other factors.

Organic photovoltaics based on inverted structures have attracted attention and are proven to be more stable than those based on conventional devices [24,25]. It is essential to enhance the quality of the interfacial layers to increase the efficiency of organic photovoltaics based on inverted structures.

Conductive polymers: Poly(3,4-ethylenedioxythiophene)-polystyrene sulfonate [26,27] and molybdenum trioxide [28,29] have been widely accepted owing to their appropriate work functions and hole extraction capabilities. Additionally, various n type electron extraction layers have been developed, such as zinc oxide [30,31], lithium fluoride [32], titanium dioxide [27] and cesium carbonate [33,34].

Zinc oxide is most commonly used in optoelectronic devices because of its appropriate work function [35], as well as superior conductivity [36], effortless processing [35] and transparency [36]. There have been several studies aiming at enhancing the performance of inverted cells using doping with a metal layer such as Al, Ga or In [37,38].

Zinc oxide is an n-type material having a wide band gap (3.3 eV) [39]. Zinc oxide becomes n type due to intrinsic defects of oxygen vacancy and the interstices occupied by excessive zinc [39]. The heat treatment atmosphere and temperature influence the thin film conductivity [40,41]. The conductivity is enhanced because of extrinsic defects on doping with Al, Ga or In. This manuscript gives a detailed account of the role of doping of ZnO interlayer with materials that enhance the device performance.

Types of modifications

Li- and Cd-doped ZnO interlayer: Kim *et al.* [47] examined the effect of doping Li and Cd in ZnO on power conversion efficiency, among other parameters. The solar parameters mentioned in literature reviewed below have been studied at stimulated air mass 1.5 global full-sun illumination. The Li-doped ZnO precursor was synthesized by dissolving zinc-acetate dihydrate and lithium-acetate dihydrate in ethanol and ethanolamine which were used as co-solvents. On the other hand, in Cd-doped ZnO precursor, zinc acetate dihydrate and cadmium nitrate tetrahydrate with the same cosolvents were used. Each of these films were spin-coated on indium tin oxide (ITO) which was used as the substrate. This was done by using the solutions at 3500 rpm for 40s, followed by drying at a temperature of 120 °C for 30 min. Finally, thermal annealing was carried out for 2 h at 450 °C. The atomic concentrations of Li and Cd in ZnO buffer layer were varied from 0 to 9.53 % and 9.02 % respectively. PTB7:$PC_{70}BM$ blend, which was the active layer, was spin-coated on the doped ZnO layers and its thickness was 85 nm. MoO_3 (thickness 10 nm) and Al electrode (thickness 100 nm) were thermally evaporated on the films after having dried them overnight under high vacuum conditions at 10^{-6} torr.

The doping action of Li in ZnO buffer layer can be due to two mechanisms, namely, substitutional doping and interstitial doping. In case of the former, Li, which acts as an acceptor, leads to decrement in carrier concentration and thus the conductivity. Lower formation energy of Li in interstitial sites as compared to substitutional sites and behaviour of Li as a good electron donor, leads to n-type doping [42]. Whereas, electrical conductivity increases by Cd-doping of ZnO buffer layer due to increase in carrier concentration, which is a result of increased oxygen vacancy (V_o) and Zn-Cd-V_o complex, which has n-type nature [43]. In case of Cd-doping, interstitial and substitutional sites act as electron donors. Both Li and Cd doping considerably increase all the solar cell parameters.

While Li-doping resulted in a short circuit current (J_{sc}) of 16.54mA/cm^2, Cd-doping gave a higher J_{sc} = 18.81 mA/cm^2, in comparison to J_{sc} = 15.80 mA/cm^2 for pristine ZnO buffer layer. Open circuit voltage (V_{oc}) and fill factor (FF) for Li-doped were 0.75 V and 59.87 %, thus giving a power conversion efficiency (PCE) of 7.46 %. Though fill factor for Cd-doping was lower (54.86 %) than in case of Li, it gave a higher V_{oc} and power conversion efficiency, which were 0.77 V and 7.90 % respectively. As mentioned earlier these parameters were also higher than those measured in undoped ZnO layer,

which had V_{oc} = 0.73V and power conversion efficiency = 5.85 %. The resistivity in Li-doped ZnO decreased until 6 atomic % concentration doping, which resulted in increment in fill factor at optimum concentration since it caused enhancement in charge extraction. The performance of organic photovoltaic improved due to Li-doping in interstitial sites, as mentioned earlier. Table-1 illustrates variation of performance parameters with the doping element.

TABLE-1
PERFORMANCE PARAMETERS OF Li-DOPED ZnO AND Cd-DOPED ZnO DEVICES [Ref. 47]

Parameters	Pristine ZnO	Li-doped ZnO (5.09 at %)	Cd-doped ZnO (5.41 at %)
J_{sc} (mA/cm^2)	15.80	16.54	18.81
V_{oc} (V)	0.73	0.75	0.77
FF (%)	50.91	59.87	54.86
PCE (%)	5.85	7.46	7.90

Another reason was the probable facilitation of electron transport in thin film transistors, which resulted due to higher electron concentration than in pristine ZnO [44]. The decrease in power conversion efficiency at 5.09 atomic % was attributed to undesirable trap formation, by excess Li dopants, within the electron extraction layer. On similar lines, enhancement of performance in case of Cd-doped ZnO buffer layer was due to resistivity reduction and higher carrier concentration. The increased V_{oc} values in both the doping cases were observed due to surface recombination suppression, a V_{oc} enhancer, owing to effective electron extraction [45,46].

Ga-doped ZnO interlayer: Shin *et al.* [48] have reported a dramatic increase in power conversion efficiency (PCE) of inverted organic photovoltaics by Ga-doped ZnO buffer layer (GZO), which acts as an electron-transport layer. The solar parameters mentioned in all the reported papers have been studied at stimulated air mass 1.5 global full-sun illumination. The device was synthesized by growing GZO nano-structured thin films employing a simple aqueous solution path, at a relatively low temperature of 90 °C. An increase of about 110 % of power conversion efficiency was observed in device with GZO as compared to undoped zinc oxide (UZO).

The synthesis of UZO and GZO thin films was carried out using a two-step solution process. The first step, which was common for both, involved seed layer preparation on indium tin oxide/glass substrate. For UZO, the seed layer was prepared on the substrate by dip-coating into 0.05 M zinc acetate dissolved in ethanol, while in case of GZO, the seed solution was prepared by dissolving gallium nitrate [$Ga(NO_3)_3 \cdot xH_2O$] and zinc acetate, in a mass ratio of 1:9, in ethanol, thus forming an n-type doping. Main growth of each layer is the second step in the synthesis. UZO layer formation was carried out in a solution of 50 mM zinc nitrate hexahydrate and 50 mM hexamethylenetetramine ($C_6H_{12}N_4$) dissolved in ethanol/deionized water (1:1 vol %) at 90 °C for 3 h. Synthesis of GZO buffer layer was carried out in the solution in which gallium nitrate (10 % mass ratio of zinc nitrate hexahydrate) was added in the solution for main growth of UZO layer. For active layer, a blend of polymers-poly(3-hexylthiophene): (6,6)-phenyl C_{61} butyric acid methyl ester, *i.e.* P3HT:PCBM, with 1:1 vol % in chlorobenzene, was spin-coated onto both buffer layers at 2000 rpm for 120 s. It was dried in covered glass dishes (*i.e.* solvent annealing [49,50]). The set-up was annealed at 150 °C for 10 min. Thermal evaporation of MoO_3 as electron blocking layer and Au anode was subsequently carried out. The thickness of GZO layers was maintained at about 270 nm.

An open circuit voltage (V_{oc}) of 0.42V was exhibited by GZO in comparison to 0.41 V of UZO buffer layer devices. The values of short circuit current (J_{sc}) and fill factor (FF) increased from 6.3 mA/cm^2 and 35.7 % in UZO to 11.7 mA/cm^2 and 39.7 % in GZO respectively. The power conversion efficiency thus showed an increase of about 110 % with reference to 0.92 % as seen in UZO. This significant enhancement of power conversion efficiency in GZO buffer layer inverted organic photovoltaics was due to improved conductivity, which resulted in higher J_{sc}.

Carbon nanostructure interface layer deposited on ZnO-nanorod arrays: Hsu *et al.* [51] in their research work studied the performance enhancement of photovoltaics by introduction of a carbon nanostructure interface layer. The solar parameters mentioned in all the papers have been studied at stimulated air mass 1.5 global full-sun illumination. This was done to overcome the problem of charge transport property at organic and inorganic junction, which affects the photovoltaic cell performance. In the experiment, oriented ZnO-nanorods were grown vertical to indium tin oxide coated glass by using hydrothermal method [52,53]. C60 powder, weighing 16 mg was dispersed in 1 mL chlorobenzene, thus forming C60 dispersion solution. The active layer used was a blend of polymers P3HT: PCBM (1:0.8 weight ratio) forming a solution in chlorobenzene at a concentration of 40 mg/mL. Fabrication of the photovoltaic device was carried out on the oriented ZnO-nanorod arrays. Having spin-coated a layer of C60 on the ZnO-nanorod arrays, the polymer blend was deposited on it. The transmission electron microscopy (TEM) image of C_{60} layer deposition on ZnO-nanorod array [50] showed that the whole structure was air-dried for one day and the film thickness was measured to be about 250 nm. Thermal deposition of a 100 nm Ag layer was carried out on top of the polymer, thus completing the device fabrication.

The short circuit current (J_{sc}) increased from 8.2 mA/cm^2, in device without carbon nanostructure to 11.6 mA/cm^2 after its introduction, while the open circuit voltage (V_{oc}) also showed an increment from 0.46 to 0.53 V. However, the fill factor (FF) remained constant, at 34 %, in both cases. To understand the above trends in greater detail, carrier motion was probed at the semiconductor-polymer interface using time resolved photoluminescence (TRPL) spectroscopy of the device before and after the insertion of C_{60} layer. The measured photoluminescence (PL) decay lifetimes were found to decrease from 208 ps, before insertion, to 150 ps after insertion of C_{60} layer. This delay in photoluminescence indicated a more efficient electron transport route, which in turn led to enhancement in photocurrent. Owing to increase in the parameters, namely, J_{sc} and V_{oc}, power conversion efficiency improved from 1.3 to 2.1 % due to insertion of C_{60} interlayer.

Dual-doped zinc oxide nano-film cathode interlayer: Using sol-gel process, Liao *et al.* [35] fabricated stable, inverted

and highly efficient polymer solar cells (PSCs). The solar parameters mentioned in all the papers have been studied at stimulated air mass 1.5 global full-sun illumination. The ZnO interlayer was doped by indium and BisNPC60-OH, which is a derivative of fullerene. This cathode interlayer was denoted as InZnO–BisC60 which was incorporated into the PSC, PTB7-Th:$PC_{71}BM$ (PTB7-Th: a polymer with low band gap [55]) being the photo absorption layer [54].

The cathode interlayer (InZnO–BisC60) contains a higher amount of fullerene derivative in the region closer to the active layer, whereas, closer to indium tin oxide, it is exuberant in indium.

The above set-up showcased better surface conductivity, which increased to 270 times the original value while in case of electron mobility it was 132 times. This led to a power conversion efficiency of 10.31 %, which was an increase of 25 % as compared to pristine ZnO.

Liao *et al.* [54,55] compared the characteristics of three doped ZnO films: InZnO-BisC60, ZnO-BisC60 and InZnO with undoped ZnO. The electronic states so formed due to doping in: InZnO, ZnO-BisC60 and InZnO-BisC60 enhanced the conductivity, in comparison to ZnO.

The devices having ZnO-BisC60 (10.31 %) and ZnO-BisC60 (9.71 %) showed improved power conversion efficiency than the ones without fullerene doping which were ZnO and InZnO. the percentage increase in power conversion efficiency was approximately 1.46 and 1.20 % respectively owing to two factors, namely: i) added pathway for the transport of electrons provided by the controlled distribution of the derivatives of fullerene on ZnO and InZnO layers and ii) the higher conduction of electrons on the bulk of the films and the surface, both of which led to efficient electron collection from the bulk of ZnO-BisC60 and In ZnO-BisC60. The above mentioned trends in parameters have been illustrated in Table-2.

Al-doped ZnO interlayer: Stubhan *et al.* [56] and Adams *et al.* [57] report high efficiency PTB7-Th:PC71BM blend-based PSCs having Al-doped cathode interlayer, prepared by spin coating. The highest efficiency 10.42 % with open-circuit voltage (V_{oc}) of 0.804 V, short-circuit current density (J_{sc}) of 17.91 mA cm^{-2} and fill factor (FF) obtained was 72.3 % with AZO interlayer with thickness of about 10 nm. Even with an interlayer of thickness 120 nm, power conversion efficiency close to 9 % was achieved. This is the highest efficiency of PSCs achieved with an interlayer having thickness more than 100 nm.

The doping concentration of Al was fixed at ≈ 1 at % to get good performance AZO [58].

The probable cause of higher current in AZO was attributed to better collection and charge transport, which consequently contributed to the enhanced J_{sc} in the inverted devices.

A ≈ 6 nm thick AZO Cathode interlayer provided a power conversion efficiency of 9.38 %. When it was increased to ≈ 10 nm, J_{sc} = 17.91 mA cm^{-2}, power conversion efficiency = 10.42 %, V_{oc} = 0.804 V and a fill factor of 72.3 %. This is one of the few studies, which present an average power conversion efficiency over 10 % for single junction PSCs [54,59,60].

Comparison of different parameters: A comparison of different parameters of the interlayers mentioned in the text has been represented in Fig. 1.

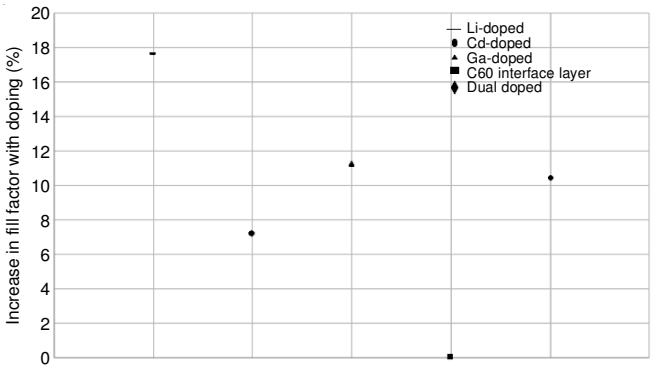

Fig. 1(a). Comparison in the increase of FF for modification in ZnO interlayers

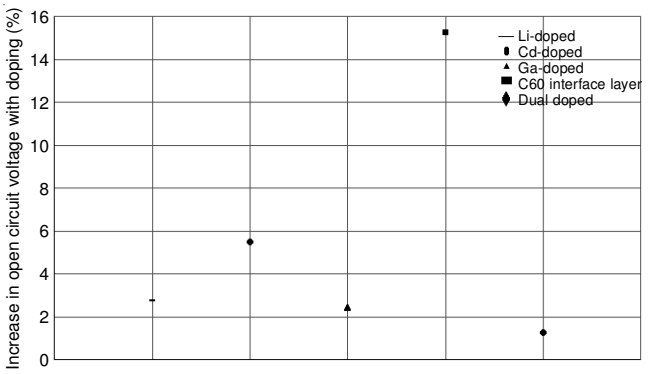

Fig. 1(b). Comparison in the increase of V_{oc} for modification in ZnO interlayers

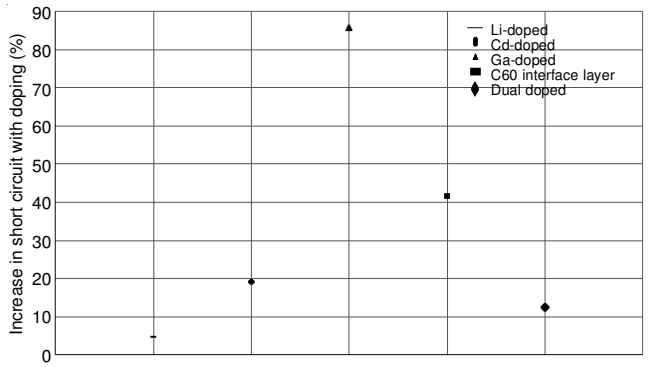

Fig. 1(c). Comparison in the increase of J_{sc} for modification in ZnO interlayers

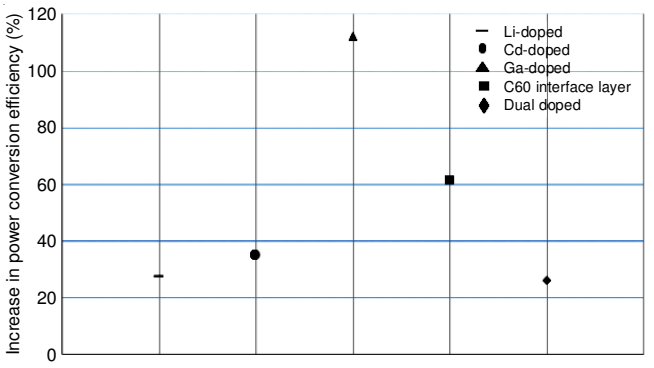

Fig. 1(d). Comparison in the increase of PCE for modification in ZnO interlayers

The gallium-doped buffer layer device showed the highest increase in power conversion efficiency, which is supported

TABLE-2
PHOTOVOLTAIC PERFORMANCE OF i-PSC BASED ON $PC_{71}BM$ [Ref. 54] WITH THE DEVICE STRUCTURE INDIUM TIN OXIDE/CATHODE INTERLAYER (40 nm)/PTB7-Th:$PC_{71}BM$ (1:1.5 w/w,100 nm)/MoO_3 (10 nm)/Ag (100 nm), (EACH PARAMETER IS AN AVERAGE OF FIVE DEVICES)

Parameters	ZnO	ZnO-BisC60	InZnO	InZnO-BisC60
J_{sc} (mA/cm^2)	15.32 ± 0.15	16.88 ± 0.12	16.32 ± 0.10	17.24 ± 0.05
V_{oc} (V)	0.79 ± 0.005	0.79 ± 0.005	0.79 ± 0.005	0.80 ± 0.005
FF (%)	67.10 ± 0.40	72.00 ± 0.30	70.00 ± 0.20	74.10 ± 0.40
PCE average (%)	8.12 ± 0.13	9.60 ± 0.11	9.03 ± 0.08	10.22 ± 0.09
PCE maximum (%)	8.25	9.71	9.11	10.31

by the fact that it also showed the highest jump in short circuit current. In case of fill factor, percentage rise was highest Li-doped buffer layer device, though the increment in short circuit current is the lowest among all others. Introduction of a C_{60} interface layer does not alter the fill factor of ZnO buffer layer, though it enhances the power conversion efficiency. Though dual doped ZnO buffer layer showed the slightest rise in power conversion efficiency, it recorded the highest value of 10.42 %.

Conclusions

In all the works reviewed above, the power conversion efficiency increased due to modification and doping of ZnO buffer layer. Zincoxide buffer layer doped with Cd showed a higher power conversion efficiency (7.90 %) than the one doped with lithium (power conversion efficiency = 7.46 %) [47]. The percentage increase in both cases as compared to pristine ZnO was 27.5 % and 35 % respectively. But power conversion efficiency showed a drop in both cases after an optimum level. In Li-doped ZnO buffer layer device, this optimum level was reached at 5.09 at%. The drop in power conversion efficiency was attributed to excess lithium dopants forming undesirable traps within the electron extraction layer, while in case of cadmium-doping, 5.41 at% was found to be the optimum level, beyond which power conversion efficiency dropped due to increasing resistivity [47].

When ZnO buffer layer was doped with Ga, the jump in power conversion efficiency was 110 % with reference to power conversion efficiency = 0.92 % of the undoped ZnO device, with a corresponding increase in fill factor from 35.7 to 39.7 %. Higher power conversion efficiency was due to improved conductivity, leading to higher J_{sc} [48]. Introduction of C60 interface layer in ZnO showed improvement in power conversion efficiency from 1.3 % to 2.1 % which was due to increase in short circuit current from 8.2 mA/cm^2 to 11.5 mA/cm^2 which in turn was a result of delay in photoluminescence [50].

Thus, Li, Cd, Ga doping and introduction of C60 interface layer in ZnO buffer layer led to increase in power conversion efficiency. The power conversion efficiency percentage increase is highest in case of Ga doping although the highest value was obtained in Cd-doping with different set-ups. In most cases, increase in electron transport layer and decrease in resistivity are the most dominant causes of higher power conversion efficiency.

In the dual doping system of InZnO-BisC60, a power conversion efficiency of 10.31 % was achieved. A champion 10.42 % was achieved in 10 nm thickness Al-doped ZnO [54-58].

ACKNOWLEDGEMENTS

The authors express their gratitude towards Institute of Chemical Technology (ICT) and General Engineering Department, ICT, Mumbai, India for providing the facilities throughout the work.

REFERENCES

1. R.E. Smalley, *MRS Bull.*, **30**, 412 (2005); https://doi.org/10.1557/mrs2005.124.
2. J. Kesters, P. Verstappen, M. Kelchtermans, L. Lutsen, D. Vanderzande and W. Maes, *Adv. Energy Mater.*, **5**, 1500218 (2015); https://doi.org/10.1002/aenm.201500218.
3. M. Hirade, H. Nakanotani, M. Yahiro and C. Adachi, *Appl. Mater. Interface*, **3**, 80 (2011); http://pubs.acs.org/doi/abs/10.1021/am100915s.
4. W.C.H. Choy, Organic Solar Cells, Materials and Device Physics, Springer-Verlag, London (2013).
5. A.F. Ali, M. Faizal and M.M. Khalil, *Phys. Lett. B*, **743**, 295 (2015); https://doi.org/10.1016/j.physletb.2015.02.065.
6. Z. He, C. Zhong, S. Su, M. Xu, H. Wu and Y. Cao, *Nat. Photonics*, **6**, 591 (2012); https://doi.org/10.1038/nphoton.2012.190.
7. K. Sun, H. Zhang and J. Ouyang, *J. Mater. Chem.*, **21**, 18339 (2011); https://doi.org/10.1039/C1JM12281A.
8. C.-H. Hsieh, Y.-J. Cheng, P.-J. Li, C.-H. Chen, M. Dubosc, R.-M. Liang and C.-S. Hsu, *J. Am. Chem. Soc.*, **132**, 4887 (2010); https://doi.org/10.1021/ja100236b.
9. Z. Xu, L.-M. Chen, G. Yang, C.-H. Huang, J. Hou, Y. Wu, G. Li, C.-S. Hsu and Y. Yang, *Adv. Funct. Mater.*, **19**, 1227 (2009); https://doi.org/10.1002/adfm.200801286.
10. M. Campoy-Quiles, T. Ferenczi, T. Agostinelli, P.G. Etchegoin, Y. Kim, T.D. Anthopoulos, P.N. Stavrinou, D.D.C. Bradley and J. Nelson, *Nat. Mater.*, **7**, 158 (2008); https://doi.org/10.1038/nmat2102.
11. L.D. Pulfry, Photovoltaic Power Generation, Van Nostrand Reinhold Co., New York, p. 230 (1978).
12. Y-W. Su, S-C. Lan and K-H. Wei, *Mater. Today*, **15**, 554 (2012); https://doi.org/10.1016/S1369-7021(13)70013-0.
13. G. Chidichimo and L. Filippelli, *Int. J. Photoenergy*, **2010**, 1 (2010); https://doi.org/10.1155/2010/123534.
14. V.S. Pathak and A. Dani, *IOSR J. Appl. Phys.*, **6**, 65 (2014).
15. M.C. Scharber and N.S. Sariciftci, *Prog. Polym. Sci.*, **38**, 1929 (2013); https://doi.org/10.1016/j.progpolymsci.2013.05.001.
16. D.W. Zhao, A.K.K. Kyaw and X.W. Sun, *Green Technol.*, **33**, 115 (2011); https://doi.org/10.1007/978-0-85729-638-2_3.
17. B. Kan, M. Li, Q. Zhang, F. Liu, X. Wan, Y. Wang, W. Ni, G. Long, X. Yang, H. Feng, Y. Zuo, M. Zhang, F. Huang, Y. Cao, T.P. Russell and Y. Chen, *J. Am. Soc.*, **137**, 3886 (2015); https://doi.org/10.1021/jacs.5b00305.
18. M.C. Scharber, D. Mühlbacher, M. Koppe, P. Denk, C. Waldauf, A.J. Heeger and C.J. Brabec, *Adv. Mater.*, **18**, 789 (2006); https://doi.org/10.1002/adma.200501717.
19. R. Pandey and R.J. Holmes, *IEEE J. Sel. Top. Quantum Electron.*, **16**, 1537 (2010); https://doi.org/10.1109/JSTQE.2010.2049256.
20. C.K. Chan, W. Zhao, A. Kahn and I.G. Hill, *Appl. Phys. Lett.*, **94**, 203306 (2009); https://doi.org/10.1063/1.3138131.
21. J. You, C.-C. Chen, Z. Hong, K. Yoshimura, K. Ohya, R. Xu, S. Ye, J. Gao, G. Li and Y. Yang, *Adv. Mater.*, **25**, 3973 (2013); https://doi.org/10.1002/adma.201300964.

22. J. You, L. Dou, K. Yoshimura, T. Kato, K. Ohya, T. Moriarty, K. Emery, C.-C. Chen, J. Gao, G. Li and Y. Yang, *Nat. Commun.*, **4**, 1446 (2013); https://doi.org/10.1038/ncomms2411.
23. J. Yu, Y. Zheng and J. Huang, *Polymers*, **6**, 2473 (2014); https://doi.org/10.3390/polym6092473.
24. M.T. Lloyd, C.H. Peters, A. Garcia, I.V. Kauvar, J.J. Berry, M.O. Reese, M.D. McGehee, D.S. Ginley and D.C. Olson, *Sol. Energy Mater. Sol. Cells*, **95**, 1382 (2011); https://doi.org/10.1016/j.solmat.2010.12.036.
25. A.K.K. Kyaw, X.W. Sun, C.Y. Jiang, G.Q. Lo, D.W. Zhao and D.L. Kwong, *Appl. Phys. Lett.*, **93**, 221107 (2008); https://doi.org/10.1063/1.3039076.
26. C.-C. Chen, W.-H. Chang, K. Yoshimura, K. Ohya, J. You, J. Gao, Z. Hong and Y. Yang, *Adv. Mater.*, **26**, 5670 (2014); https://doi.org/10.1002/adma.201402072.
27. J.Y. Kim, K. Lee, N.E. Coates, D. Moses, T.-Q. Nguyen, M. Dante and A.J. Heeger, *Science*, **317**, 222 (2007); https://doi.org/10.1126/science.1141711.
28. P. Schulz, S.R. Cowan, Z.-L. Guan, A. Garcia, D.C. Olson and A. Kahn, *Adv. Funct. Mater.*, **24**, 701 (2014); https://doi.org/10.1002/adfm.201302477.
29. S.R. Hammond, J. Meyer, N.E. Widjonarko, P.F. Ndione, A.K. Sigdel, A. Garcia, A. Miedaner, M.T. Lloyd, A. Kahn, D.S. Ginley, J.J. Berry and D.C. Olson, *J. Mater. Chem.*, **22**, 3249 (2012); https://doi.org/10.1039/c2jm14911g.
30. L.K. Jagadamma, M. Al-Senani, A. El-Labban, I. Gereige, G.O. Ngongang Ndjawa, J.C.D. Faria, T. Kim, K. Zhao, F. Cruciani, D.H. Anjum, M.A. McLachlan, P.M. Beaujuge and A. Amassian, *Adv. Energy Mater.*, **5**, 1500204 (2015); https://doi.org/10.1002/aenm.201500204.
31. M.S. White, D.C. Olson, S.E. Shaheen, N. Kopidakis and D.S. Ginley, *Appl. Phys. Lett.*, **89**, 143517 (2006); https://doi.org/10.1063/1.2359579.
32. C.J. Brabec, S.E. Shaheen, C. Winder, N.S. Sariciftci and P. Denk, *Appl. Phys. Lett.*, **80**, 1288 (2002); https://doi.org/10.1063/1.1446988.
33. C.-I. Wu, C.-T. Lin, Y.-H. Chen, M.-H. Chen, Y.-J. Lu and C.-C. Wu, *Appl. Phys. Lett.*, **88**, 152104 (2006); https://doi.org/10.1063/1.2192982.
34. G. Li, C.W. Chu, V. Shrotriya, J. Huang and Y. Yang, *Appl. Phys. Lett.*, **88**, 253503 (2006); https://doi.org/10.1063/1.2212270.
35. Y. Sun, J.H. Seo, C.J. Takacs, J. Seifter and A.J. Heeger, *Adv. Mater.*, **23**, 1679 (2011); https://doi.org/10.1002/adma.201004301.
36. O. Tari, A. Aronne, M.L. Addonizio, S. Daliento, E. Fanelli and P. Pernice, *Sol. Energy Mater. Sol. Cells*, **105**, 179 (2012); https://doi.org/10.1016/j.solmat.2012.06.016.
37. H. Oh, J. Krantz, I. Litzov, T. Stubhan, L. Pinna and C.J. Brabec, *Sol. Energy Mater. Sol. Cells*, **95**, 2194 (2011); https://doi.org/10.1016/j.solmat.2011.03.023.
38. M. Thambidurai, J.Y. Kim, C.-M. Kang, N. Muthukumarasamy, H.-J. Song, J. Song, Y. Ko, D. Velauthapillai and C. Lee, *Renew. Energy*, **66**, 433 (2014); https://doi.org/10.1016/j.renene.2013.12.031.
39. A.K.K. Kyaw, Y. Wang, D.W. Zhao, Z.H. Huang, X.T. Zeng and X.W. Sun, *Phys. Status Solidi (a)*, **208**, 2635 (2011); https://doi.org/10.1002/pssa.201127263.
40. G. Gonçalves, E. Elangovan, P. Barquinha, L. Pereira, R. Martins and E. Fortunato, *Thin Solid Films*, **515**, 8562 (2007); https://doi.org/10.1016/j.tsf.2007.03.126.
41. G. Gonçalves, E. Elangovan, P. Barquinha, L. Pereira, R. Martins and E. Fortunato, *Thin Solid Films*, **515**, 8562 (2007); https://doi.org/10.1016/j.tsf.2007.03.126.
42. C.H. Park, S.B. Zhang and S.-H. Wei, *Phys. Rev. B*, **66**, 073202 (2002); https://doi.org/10.1103/PhysRevB.66.073202.
43. X. Tang, H. Lü, Q. Zhang, J. Zhao and Y. Lin, *Solid State Sci.*, **13**, 384 (2011); https://doi.org/10.1016/j.solidstatesciences.2010.11.040.
44. P. Nayak, J. Jang, C. Lee and Y. Hong, *J. Soc. Inf. Disp.*, **18**, 552 (2010); https://doi.org/10.1889/JSID18.8.552.
45. W. Tress, N. Marinova, O. Inganäs, M.K. Nazeeruddin, S.M. Zakeeruddin and M. Graetzel, *Adv. Energy Mater.*, **5**, 1400812 (2014); https://doi.org/10.1002/aenm.201400812.
46. G. Li, M. Liang, H. Wang, Z. Sun, L. Wang, Z. Wang and S. Xue, *Chem. Mater.*, **25**, 1713 (2013); https://doi.org/10.1021/cm400196w.
47. J. Y. Kim, J. Kim, J. Roh, H. Kim, C. Lee, *IEEE J. Photovoltaics*, 6, 930 (2016); https://doi.org/10.1109/JPHOTOV.2016.2553780.
48. K.-S. Shin, K.-H. Lee, H.H. Lee, D. Choi and S.-W. Kim, *J. Phys. Chem. C*, **114**, 15782 (2010); https://doi.org/10.1021/jp1013658.
49. G. Li, V. Shrotriya, J. Huang, Y. Yao, T. Moriarty, K. Emery and Y. Yang, *Nat. Mater.*, **4**, 864 (2005); https://doi.org/10.1038/nmat1500.
50. G. Li, Y. Yao, H. Yang, V. Shrotriya, G. Yang and Y. Yang, *Adv. Funct. Mater.*, **17**, 1636 (2007); https://doi.org/10.1002/adfm.200600624.
51. F.-C. Hsu, C.-T. Chen, Y.-M. Sung and Y.-F. Chen, *IEEE*, 716-718 (2011); https://doi.org/10.1109/PVSC.2011.6186054.
52. M. Ohyama, H. Kouzuka and T. Yoko, *Thin Solid Films*, **306**, 78 (1997); https://doi.org/10.1016/S0040-6090(97)00231-9.
53. L. Vayssieres, *Adv. Mater.*, **15**, 464 (2003); https://doi.org/10.1002/adma.200390108.
54. S.-H. Liao, H.-J. Jhuo, P.-N. Yeh, Y.-S. Cheng, Y.-L. Li, Y.-H. Lee, S. Sharma and S.-A. Chen, *Sci. Rep.*, **4**, 6831 (2014); https://doi.org/10.1038/srep06813.
55. S.-H. Liao, H.-J. Jhuo, Y.-S. Cheng and S.-A. Chen, *Adv. Mater.*, **25**, 4766 (2013); https://doi.org/10.1002/adma.201301476.
56. T. Stubhan, I. Litzov, N. Li, M. Salinas, M. Steidl, G. Sauer, K. Forberich, G.J. Matt, M. Halik and C.J. Brabec, *J. Mater. Chem. A Mater. Energy Sustain.*, **1**, 6004 (2013); https://doi.org/10.1039/c3ta10987a.
57. J. Adams, M. Salvador, L. Lucera, S. Langner, G.D. Spyropoulos, F.W. Fecher, M.M. Voigt, S.A. Dowland, A. Osvet, H.-J. Egelhaaf and C.J. Brabec, *Adv. Energy Mater.*, **5**, 1501065 (2015); https://doi.org/10.1002/aenm.201501065.
58. X. Liu, X. Li, Y. Li, C. Song, L. Zhu, W. Zhang, H.-Q. Wang and J. Fang, *Adv. Mater.*, **28**, 7405 (2016); https://doi.org/10.1002/adma.201601814.
59. Z.C. He, B. Xiao, F. Liu, H.B. Wu, Y.L. Yang, S. Xiao, C. Wang, T.P. Russell and Y. Cao, *Nat. Photonics*, **9**, 174 (2015); https://doi.org/10.1038/nphoton.2015.6.
60. L. Nian, W.Q. Zhang, S.P. Wu, L.Q. Qin, L.L. Liu, Z.Q. Xie, H.B. Wu and Y.G. Ma, *ACS Appl. Mater. Interfaces*, **7**, 25821 (2015); https://doi.org/10.1021/acsami.5b07759.